minerals

MDPI

Article

Leaching Behavior and Mineralogical Control of Heavy Metal Elements in Bauxite Under High Sulphate Acid Mine Drainage Conditions

Sékou Mohamed Condé [1,2], Xiujuan Feng [1,2,3,4,*] and Xinglong Zhao [1]

[1] School of Mines, China University of Mining and Technology, Xuzhou 221116, China; sekoumohamedconde1@gmail.com (S.M.C.); xinglongzhao@cumt.edu.cn (X.Z.)
[2] Guizhou Provincial Academician Workstation for Efficient Exploitation of Rich Mineral Resources and Environmental Protection, Guiyang 550081, China
[3] State Key Laboratory for Safe Mining of Deep Coal Resources and Environment Protection, Anhui University of Science and Technology, Huainan 232001, China
[4] Guizhou Rongyuan Environmental Protection Technology Co., Ltd., Guiyang 550081, China
* Correspondence: fengxj.2011@tsinghua.org.cn

Abstract

Shanxi Province in China is one of the world's major bauxite producers. The co-existence of coal and bauxite mining makes this province particularly prone to acid mine drainage (AMD) and, thus, a significant area for investigating heavy metal mobility in an aluminum-rich geological environment. In this study, heavy metal leaching from bauxite under simulated AMD conditions and the geochemical mechanisms controlling their mobility were examined in this study. XRF analysis demonstrated that the bauxite is predominantly composed of Al_2O_3, Fe_2O_3 and SiO_2, while XRD, FTIR, and SEM-EDS revealed that diaspore and kaolinite dominate bauxite, together with accessory Fe- and Ti-bearing phases, providing reactive surfaces for adsorption and precipitation. After batch leaching with synthetic acidic sulphate solutions (pH = 3), $Ca(OH)_2$ neutralization was regulated. The data reveal that pH is the key factor controlling heavy metal mobility. Acidic conditions enhanced metal release while alkaline conditions favored hydroxide precipitation, surface complexation and co-precipitation. The removal efficiency was 91%–99% for Cd and Zn, 100% for Cd and Zn, 69%–90% for Cr, 35%–100% for Cu, 92%–100% for Ni and up to 100% for Pb. The chemical and mineralogical composition played an indirect role by providing adsorption sites but did not prevent the release of metals under acidic conditions. These results reveal that pH adjustment is the major mechanism controlling heavy metal immobilization in AMD-impacted bauxite systems and contributes to the knowledge of geochemical processes controlling metal mobility in acidic mine drainage.

Keywords: bauxite; acid mine drainage; heavy metals leaching; mineralogical characterization; geochemical processes; alkaline regulation

Check for updates

Academic Editors: Yinxian Song, Yubo Wen, Saglara S. Mandzhieva and Niloofar Karimian

Received: 31 May 2026
Revised: 11 July 2026
Accepted: 27 July 2026
Published: 4 August 2026

Copyright: © 2026 by the authors. Licensee MDPI, Basel, Switzerland. This article is an open access article distributed under the terms and conditions of the Creative Commons Attribution (CC BY) license.

1. Introduction

Bauxite is an important component of non-ferrous metals, with considerable relevance for the production of aluminum products, and also plays a significant part in the development and utilization of mineral resources [1,2]. The bauxite studied is white-to-light-gray in color, typical of several diasporic bauxite deposits in China. In contrast, most deposits of bauxite around the world are typically red-to-reddish-brown because of their higher

iron oxide content, with a relative density of 2.32 to 2.42 g/cm^3. Laterite, karst, or sedimentary are the classifications based on the changes in the underlying substrate. The composition includes aluminum-containing minerals (gibbsite, boehmite, and/or diaspore), iron-containing minerals (mostly hematite and goethite), and trace amounts of silicate, titanite, sulphate, and carbonate [3–5]. Prospection and exploration indicate that bauxite deposits are widely distributed worldwide; nevertheless, economically significant reserves are concentrated in particular places, notably West Africa (Guinea), Northern-Southwestern of Australia, Northern-South of America, and some areas of Asia. Lateritic bauxite is widely distributed in tropical and subtropical regions from 0° to 30° north latitude. Lateritic bauxite is mostly soft aluminum ore, the best material for smelting aluminum, and is found in Africa, Oceania, Latin America, and Southeast Asia [6–8]. Karst-type bauxite is predominantly composed of diaspore and is typically characterized by high-grade aluminum content and is found in the Caribbean, Southern European Sea, and northern Asia [9–14]. Sedimentary bauxite deposits are generally smaller in scale and exhibit more variable mineral composition, and are primarily distributed in China and Eastern and Central Europe [15,16].

China has rich bauxite resources, with estimated total reserves of 2.29 billion tons, ranking 7th in the world [17–19]. China is the largest aluminum producer and has had remarkable expansion in its aluminum sector throughout the last 30 years. China overtook the United States in aluminum output to become the world's top aluminum producer in 2002, according to figures from the International Aluminum Association [20]. The rapid growth of industry and increasing demand for aluminum have resulted in significant developments of its bauxite mining industry, which have been extensively studied in the scholarly literature [21,22]. Bauxite deposits in China are primarily distributed in Shanxi (mainly Luliang and Xinzhou), Guizhou (mainly Guiyang and Zunyi), Henan (mainly for Sanmenxia, Luoyang, Zhengzhou, Pingdingshan and other places), and Guangxi provinces (mainly Baise and Guigang) [23]. These regions account for 41.7%, 17.8%, 16.6%, and 15.8% of the nation's total estimated reserves, respectively. Furthermore, small bauxite resources are also found in provinces including Yunnan, Shandong, Chongqing, Hainan and Sichuan, but their cumulative reserves account for less than 10% of the national total [24–31].

Soil heavy metal pollution has been an increasing environmental concern with the increased development of economic activity [32]. Heavy metals are highly persistent and poisonous. They have the ability to penetrate crops and vegetables, thereby representing a concern to human health. The mining industry is considered as a great contributor to high levels of toxic elements in the environment [33], and also to the accumulation of heavy metals in plants grown in soils irrigated with water from rivers contaminated with mine water [34]. To understand the mineralogical characteristics, leaching dynamics and processing efficiency of bauxite with exchangeable and surface-bound heavy metal fractions [35], a comprehensive examination of the pore structure of bauxite, which governs fluid flow and ion migration within the mineral structure, is necessary. Lateritic bauxites, in particular, can be very porous due to intense weathering processes, but karstic bauxites tend to have more complex pore porous structures [36]. The features of these pores have a strong influence on the physical and chemical properties of the ore and hence on leaching efficiency and metal mobility [12]. During leaching, the leaching agents react with mineral phases and tiny particles migrate and redistribute, thereby changing the pore shape and connectivity [37]. The porosity of the ore governs the contact surface between the leaching solution and the mineral surfaces, which in turn directly influences the reaction kinetics, the ion exchange processes, and the mass transfer efficiency [38,39]. Hence, pore structure is significant to limit the release and retention of heavy metals in bauxite in the case of

AMD [40,41]. Several studies [42–45] have reported environmental damage due to heavy metal discharge through AMD.

AMD is a substantial worldwide environmental concern at mining sites, primarily resulting from sulfide oxidation. It is produced by the chemical reaction between sulfide minerals exposed to the air and water deposited on it, which forms sulfuric acid [42]. AMD is distinguished by its low pH and the presence of a variety of high concentrations of heavy metals that are leached from mineral materials that have been exposed to acid. AMD poses a threat to the ecosystem, destroys the natural habitat of animals, and results in the loss of biodiversity in proximity to the mining site [46]. In addition to sulfide minerals, mining wastes may contain more mineral phases that might protect acidity, neutralize acid mine drainage, or promote the immobilization of dissolved metals, thus mitigating their geochemical interactions with the environment. These minerals are principally carbonates, clay minerals, metal oxides, hydrated salts, phosphates, arsenates and native elements [43,47]. High amounts of copper pose risks to aquatic and terrestrial ecosystems and to human health [45]. Ingesting fish from rivers polluted with mine water [44] poses a health risk for fish populations and for humans who consume them, due to the bioaccumulation of trace elements (As, Cd, Cr, Ni, Cu, Pb, Zn, Pt) in edible fish species [43,48], and to the accumulation of heavy metals in plants cultivated in soils irrigated with water from these polluted rivers [43].

The bauxite samples were collected from Aojiawan mining area in Xing Country, Shanxi Province, China (Figure 1), a region characterized by significant diasporic bauxite deposits [17,19]. Shanxi is one of the major mining provinces in China, where coal and bauxite resources frequently coexist within the same geological formations [23,28]. The mining area is located in the Northeastern boundary of Luliangshan mountain chain, in the Weifen River watershed of the Yellow River Basin. The typical topography of the region is characterized by Loess erosion, with deep gullies and steep relief. Bedrock exposure is limited because approximately 90% of the area is covered by Quaternary loess and Tertiary laterite. Vegetation is limited in the mining area. Bauxite exists in the middle and lower Carboniferous Benxi Formation iron clay rocks and Shanxi-type iron ore. The mining background is environmentally significant because large-scale coal mining in the region has been linked to AMD generation, which poses a severe threat to local water systems and ecosystems [40,41].

Previous studies have shown that AMD is a common problem in Shanxi, which is attributed to the oxidation of sulfide minerals in coal-bearing strata, producing acidic, metal-rich drainage that can interact with the surrounding geological materials [42,49]. While direct AMD discharge was not analyzed in this study, the geological and mining conditions of the area offer a realistic and representative framework for examining the interaction between acidic sulphate waters and bauxite. Consequently, simulated AMD treatments were taken on to replicate such conditions in controlled laboratory environments.

AMD is an undesirable result of mining activities and most of the research on this topic is based on the bad consequences of mining activities with the possible advantages being ignored. Only a few research studies have thoroughly investigated the combined effect of mineralogical composition and sulphate-rich AMD conditions on the leaching behavior of heavy metals in diasporic bauxite systems.

This study aims to analyze the relationship between the mineralogical composition of bauxite and the environmental leaching behavior of heavy metals simulating AMD conditions. The main objectives are to: (i) characterize the mineralogical composition of bauxite by using advanced analytical techniques such as XRD, SEM-EDS and FTIR; (ii) assess the leaching behaviors of heavy metals under simulated AMD conditions; (iii) investigate the influence of pH neutralization (by addition of Ca $(OH)_2$) on the mechanisms of metal

immobilizations; and (iv) understand the geochemical mechanisms that control metal release and retention in bauxite. This work evaluates geochemical processes controlling metal mobility in aluminum-rich geological environments impacted by mine drainage, which is relevant to environmental risk assessment and mine water management in bauxite mining regions.

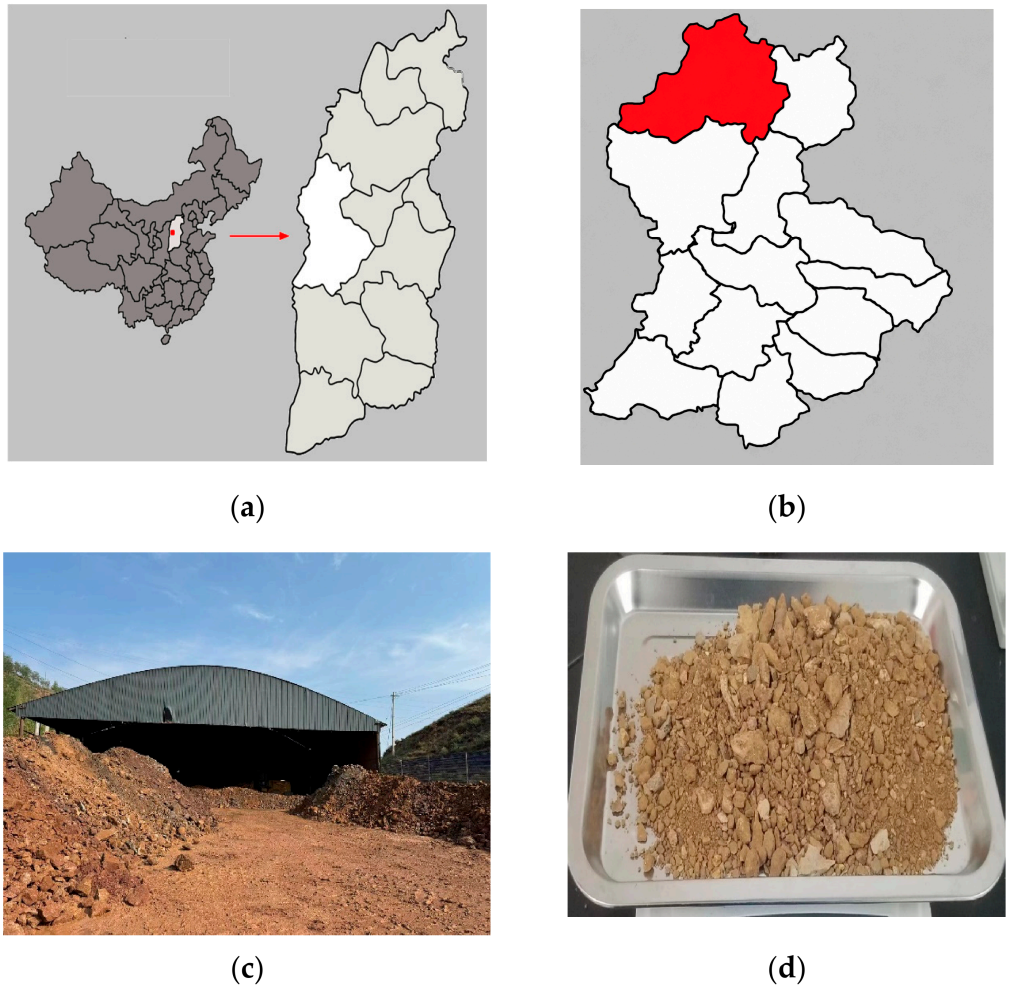


Figure 1. Map of studied area: (**a**) location of Lüliang Prefecture within Shanxi (China); (**b**) China Luliang Xing. (**c**) Aojiawan No. 1 Bauxite mine, and Aojiawan No. 2 Bauxite mine; (**d**) sample of bauxite.

2. Materials and Methods

2.1. Bauxite Samples Collection, and Characterization Physicochemical Analysis

The bauxite sample were collected from Aojiawan No. 1 Bauxite mine, and Aojiawan No. 2 Bauxite mine in Shanxi Province, China with gray appearance and uneven particle size distribution. The ore sample is characterized by the presence of dispersed and irregular particles, ranging in diameter from less than 0~−1.43 mm. The collected ore samples were collected at different points, mixed evenly to obtain a composite sample, transported to the laboratory and stored in the dark. Visible impurities such as plant debris, loose soil particles and other foreign items were removed manually. The ore samples were oven-dried at 105 °C for a duration of 12 h, and passed through a 10-mesh sieve for further chemical analyses and leaching experiments.

The pseudo-total concentrations of heavy metals were determined using microwave-assisted aqua regia digestion method according to ISO 12914:2012 (Soil Quality-Microwave-assisted extraction of the aqua regia soluble fraction for the detection of elements. Inter-

national Organization for Standardization (ISO): Geneva, Switzerland, 2012) [50]. This extraction technique is designed to target the aqua regia soluble (pseudo-total) portion of metals and not the refractory silicate bound phases and consequently gives an approximation of the environmentally accessible metal pool.

The dried materials were finely powdered, homogenized and sieved with a 200 mesh (75 μm) sieve for chemical analysis. About 0.2 g of the homogenized powder was put into a microwave digestion vessel and digested with an aqua regia mixture (HCl-HNO_3) under controlled microwave heating for 2 h. Each sample was produced and analyzed in duplicate to evaluate analytical repeatability. The digested solutions were cooled, filtered, if necessary, quantitatively transferred to volumetric flasks and diluted with deionized water to a known volume and analyzed for As, Cd, Cr, Cu, Ni, Pb and Zn by inductively coupled plasma optical emission spectrometry (ICP-OES).

2.2. Mineralogical Characterization

2.2.1. X-Ray Fluorescence (XRF) Analysis

The chemical composition of the bauxite samples was evaluated by X-ray fluorescence (XRF) using a Zetium X-ray fluorescence spectrometer (Malvern Panalytical B.V., Almelo, The Netherlands). Before analysis the samples were dried, finely powdered and formed as pressed powder pellets using the pelletizing process without fusion. Homogeneous pellets were obtained by mixing around 0.6 g of sample powder with microcrystalline cellulose as a binder and pressing at room temperature (about 25 °C) at 30 t for 45 s. Qualitative and semi-quantitative analyses were carried out by the Omnian-30 standardless analysis tool included with the device. The XRF spectrometer was operated at the maximum power of 2.4 kW and excitation settings were automatically tuned according to the element range (25–60 kV and 40–96 mA). The elemental composition was then stated in both elemental and oxide form.

2.2.2. X-Ray Diffractometer (XRD) Analysis

The mineral composition of bauxite samples was evaluated by X-ray diffraction (XRD) using a D8 Advance X-ray diffractometer (Bruker AXS GmbH, Karlsruhe, Germany) with a Cu Kα radiation source (λ = 1.5406 Å). The equipment was used at 40 kV and 30 mA. The diffraction patterns were recorded over a 2θ range of 5–70° with a step size of 0.01945° and a counting time of 0.07–0.20 s per the step. The resulting test data is processed and analyzed using MDI jade 6 software.

2.2.3. Scanning Electron Microscopy and Energy Dispersive Spectroscopy (SEM-EDS) Analysis

Scanning electron microscopy (SEM) is a frequently utilized technique for the examination and evaluation of the surface morphology of materials. The surface morphology and microstructural features of the bauxite samples were studied using a Quattro S field-emission scanning electron microscope (FE-SEM) with an energy-dispersive X-ray spectroscopy (EDS) system (FEI Company, Brno, Czech Republic; model M0AIA3 LMH). SEM observations were performed at an accelerating voltage of 10.0 kV, working distance of 4.91 mm, and magnification of 5000×. Secondary electron pictures were obtained using an In-Beam SE detector (FEI Company, Brno, Czech Republic). For SEM-EDS investigation, the samples were analyzed without conductive coating.

2.2.4. Infrared Spectrometer (FT-IR)

The functional groups and chemical bonds of the mineralogical elements of the bauxite samples were identified using Fourier-transform infrared (FT-IR) spectroscopy. FT-IR investigations were performed with a VERTEX 80 V Fourier-transform infrared spec-

trometer (Bruker Optics, Ettlingen, Germany) in transmission mode with a deuterated triglycine sulphate (DTGS) detector. All spectra were acquired in the wavenumber range of 4000–400 cm^{-1} with a spectral resolution of 4 cm^{-1}, based on 32 scans per sample using the MIR_TR.XPM experiment protocol. The samples were analyzed as fine powdered powders. The FT-IR spectra obtained were analyzed with the XRD data, to find the distinctive functional groups and to confirm the mineralogical composition of the bauxite samples [51].

2.3. Leaching Experiment Design

2.3.1. Preparation of Simulated Leaching Solutions of AMD

To simulate AMD conditions, synthetic leaching solutions were formulated based on the typical geochemical characteristics of mine drainage from coal mines in northern China and similar mining environments [40,42,49]. These solutions were prepared by mixing sulfuric acid (H_2SO_4) and sodium sulfate (Na_2SO_4) in deionized water, thereby allowing independent regulation of both acidity (pH) and sulfate (SO_4^{2-}) concentration. Hydrochloric acid and sodium hydroxide (NaOH) were used to adjust the pH of the leaching solution. The temperature was kept at 25 °C. Such systems are typically low pH (3) and have high sulphate concentrations, which arise from the oxidation of sulfide minerals such as pyrite. In all studies, the baseline pH and the sulphate concentration were held constant to isolate the influence of Ca $(OH)_2$ dosage on metal removal and geochemical processes. Each solution was produced in a 1000 mL volumetric flask with ultrapure deionized water. The required pH was attained by slowly adding exact quantities of concentrated sulfuric acid while constantly stirring. The pH was tested at the end with a calibrated pH meter. The appropriate sulphate concentrations were obtained by adding sodium sulphate (Na_2SO_4, >99% purity). This phase was to mimic the amounts of sulphate in AMD. The exact amount of Na_2SO_4 was weighed on an analytical balance and then added to the acidified solution. All solutions were thoroughly mixed and stored in plastic bottles that had been previously washed with acid until use. This simplified composition allows for controlled investigation of the effects of acidity and sulphate on heavy metal leaching and mineral solution interactions.

2.3.2. Batch Leaching Experimental Procedure, pH Levels, Liquid-to-Solid-Ratio

The leaching absorption experiments were conducted in batch mode under controlled laboratory conditions to simulate the interaction between acid mine water, bauxite, and removed chemical substances. The aim was to assess mobilization of heavy metals (As, Cd, Cu, Ni, Pb, Zn) under varying pH and sulphate concentrations. A mass of 4.00 g of bauxite was used for each leaching test. The sample was randomly put in the batch of leaching and synthetic leaching solutions were added. Acid mine water was generated from H_2SO_4 and Na_2SO_4 and the extracted chemical compounds were added in proper proportions. For each test, 40.0 mL of leaching solution was applied to the solid sample with L/S ratio of 10:1. The bauxite-solution mixture was transferred to acid-washed polypropylene centrifuge tubes, which were sealed to reduce evaporation, and agitated with a shaker (THZ-82A) at an oscillation speed of 200 rpm and a constant temperature of 25 °C for a duration of 24 h. Subsequent to leaching, the suspension was centrifuged for 15 mn at 4000 rpm, and the supernatant was filtered using a membrane filter (15–20 μm). The digests were analyzed using ICP-OES to ascertain the amounts of heavy metals in the solution.

However, the present study was designed as a short-term batch experiment intended to investigate the initial geochemical response of heavy metals in bauxite under simulated AMD conditions. The selected contact time was chosen to achieve near-equilibrium laboratory conditions and to identify dominant dissolution, adsorption, and precipitation mechanisms. Therefore, the experimental results should be interpreted as short-term

geochemical behavior and not as a direct representation of long-term field-scale AMD processes occurring at mining sites.

2.3.3. Analytical Methods

Dissolved heavy metal concentrations were determine (ICP-OES HKYT-799; Beijing Huake Yitong Analytical Instrument Co., Ltd., Beijing, China). The pH and electrical conductivity (EC) of the leachate were assessed post-filtration utilizing a calibrated pH meter (PHS-3C) and a conductivity meter (DDS-11A; Shanghai Yueping Scientific Instrument Co., Ltd., Shanghai, China). Calibration was performed daily with standard buffer solutions (pH 4.00, 9.18) and KCl standards for electrical conductivity (EC).

2.4. Neutralization Process (Liming)

Following the acid leaching testing, neutralization tests were performed using calcium hydroxide (Ca $(OH)_2$ purity $\geq$ 95.0%; Xilong Scientific Co., Ltd., Shantou, China) to simulate the alkaline treatment usually utilized for the remediation of AMD. Specific concentrations of Ca $(OH)_2$ (0.1 to 1.0 g, which corresponded to 0.014 to 0.14 mol/L of each treatment agent variation with 2%, 3% and 5% w/v) were immediately added to the leached bauxite suspension. The mixtures were agitated at 200 rpm and kept at 25 °C for 24 h to allow appropriate reaction and equilibrium.

The pH of the system was measured with a calibrated pH meter (PHS-3C) and methodically adjusted to the desired values in the range from neutral to severely alkaline conditions (pH 7–12). The samples were treated, centrifuged, filtered and then chemically analyzed. This method enabled us to evaluate the effect of high pH on the precipitation, adsorption and coprecipitation processes of heavy metals.

2.5. Data Treatment and Statistical Analysis

The concentrations of dissolved heavy metals (As, Cd, Cr, Cu, Ni, Pb, and Zn) in the leachates were determined by ICP-OES. All experiments were carried out in duplicate, with some in quintuplicate; the data is represented as mean values $\pm$ standard deviation. Initial data processing, organization and tabulation was done in Excel 2019. Origin Pro 2021 was used to generate figures. The rigorous analytical approach ensured the accuracy of the analysis and interpretation of the datasets.

Leaching performance was expressed as removal efficiency (R, %). The removal efficiency was calculated by the following equation:

$$R\% = \frac{C_0 - C_t}{C_0} \times 100 \quad (1)$$

where: C_0 is the initial concentration of the metal in the solution before treatment (mg/L) and C_t is the concentration of the metal in the solution after leaching or neutralization (mg/L).

Positive R values indicate a net removal of metals from the aqueous phase, while negative values indicate a net release of metals into the solution, through desorption or mineral dissolution processes. In highly acidic and sulphate-rich matrices, ICP-OES analysis has several problems determining trace-level concentrations. High ionic strength and dissolved sulphate concentrations can change plasma stability, emission intensity, and analytical precision due to matrix effects. Also, overlapping emission wavelengths can cause spectral interferences, which might cause small mistakes, especially for ultra-trace elements. Calibration standards, repeated analyses, and quality-control systems reduced analytical uncertainty, but instrumental variability remains.

3. Results

3.1. Mineralogical Characteristics of Bauxite

3.1.1. Chemical Composition by XRF

The chemical composition of the bauxite sample collected by XRF is presented in Table 1. The results revealed that the sample is mostly composed of Al_2O_3 (46.45 wt%), Fe_2O_3 (25.06 wt%) and SiO_2 (19.44 wt%) and the other oxides are in the relatively low proportions. The primary elements as elemental form are aluminum (36.90 wt%), iron (36.46 wt%) and silicon (15.04 wt%), confirming that the material studied is an alumina-rich, iron-bearing diasporic bauxite.

Table 1. Chemical composition.

Oxide	Content (wt%)
Al_2O_3	46.45
Fe_2O_3	25.06
SiO_2	19.44
TiO_2	3.36
CaO	2.51
K_2O	1.77
and others	<1

This high proportion of Al_2O_3 is in consistent agreement with the mineralogical composition observed by XRD and FTIR. The predominant aluminum mineral was diaspore (AlO(OH)) along with kaolinite ($Al_2Si_2O_5(OH)_4$). The presence of 19.44 wt% SiO_2 is consistent with the quantity of kaolinite as reflected by the diffraction peaks and the characteristic FTIR absorption bands at 1024 cm^{-1} and 914 cm^{-1}, indicating that aluminosilicate minerals form a large part of the bauxite matrix.

The studied sample is characterized by a relatively high content of Fe_2O_3, which reveals that iron-bearing minerals are an important portion of the ore. The main crystalline phases were determined by XRD examination. SEM-EDS elemental maps revealed a broad distribution of Fe in the mineral matrix. Iron occurs as independent accessory minerals and as fine disseminations associated with aluminosilicates. Such Fe-bearing phases are environmentally relevant, as iron oxides and oxyhydroxides are characterized by high specific surface area and a large number of reactive hydroxyl groups that can adsorb trace metals through surface complexation and co-precipitation processes. Therefore, they are anticipated to play a significant role in immobilizing heavy metals during AMD leaching.

The sample additionally has a 3.36 wt% TiO_2 indicating presence of titanium-carrying accessory minerals, most likely rutile or anatase, but their abundance may be too low to be identified clearly by XRD. This is also consistent with the localized Ti enrichment in the SEM-EDS elemental distribution. Such behavior has been reported repeatedly for diasporic bauxites in which Ti-bearing minerals occur as minor accessory phases in intimate association with aluminum minerals.

The minor oxides include CaO (2.51 wt%), K_2O (1.77 wt%), MgO (0.36 wt%), MnO (0.27 wt%), P_2O_5 (0.12 wt%) and SO_3 (0.08 wt%) with a total less than 5 wt% of the bulk composition. In very small concentrations, these components could locally influence mineral dissolution, ion exchange and secondary mineral precipitation when affected by AMD.

Trace-element oxides, such as Cr_2O_3 (0.05 wt%), NiO (0.04 wt%), Co_3O_4 (0.07 wt%), PbO (0.03 wt%), ZrO_2 (0.17 wt%), Y_2O_3 (0.03 wt%), Nb_2O_5 (0.02 wt%) and SrO (0.16 wt%), are present only in small amounts. These elements are of small abundance but are environmentally significant as they may be liberated during acid weathering and contribute

to trace-metal pollution. The mineralogical affinities, pH and subsequent adsorption or precipitation reactions during AMD leaching would likely strongly influence their mobility.

Overall, the XRF results are in excellent agreement with the XRD, FTIR and SEM–EDS investigations, which demonstrate that the investigated bauxite is a diasporic ore of iron-rich aluminosilicates dominated by aluminum hydroxides, clay minerals and accessory Fe- and Ti-bearing phases. This mineralogical and geochemical background is used to evaluate the following leaching behavior and immobilization mechanisms of heavy metals under simulated AMD circumstances.

Chemical composition of bauxite was first established by XRF for general elemental chemistry and then mineralogical characterization by XRD, FTIR and SEM-EDS methods.

3.1.2. Mineralogical Characterization by XRD

The crystalline mineral phases in bauxite sample taken from Shanxi Province, northern China were identified by X-ray diffraction (XRD) after bulk chemical characterization by XRF. The lithology of the bauxite layer is generally characterized by dominance of some minerals, and the optical microscope observation provides the basis for further research. The diffraction pattern presented in Figure 2 reveals well defined peaks indicating a high degree of crystallinity and relatively simple mineralogical composition.

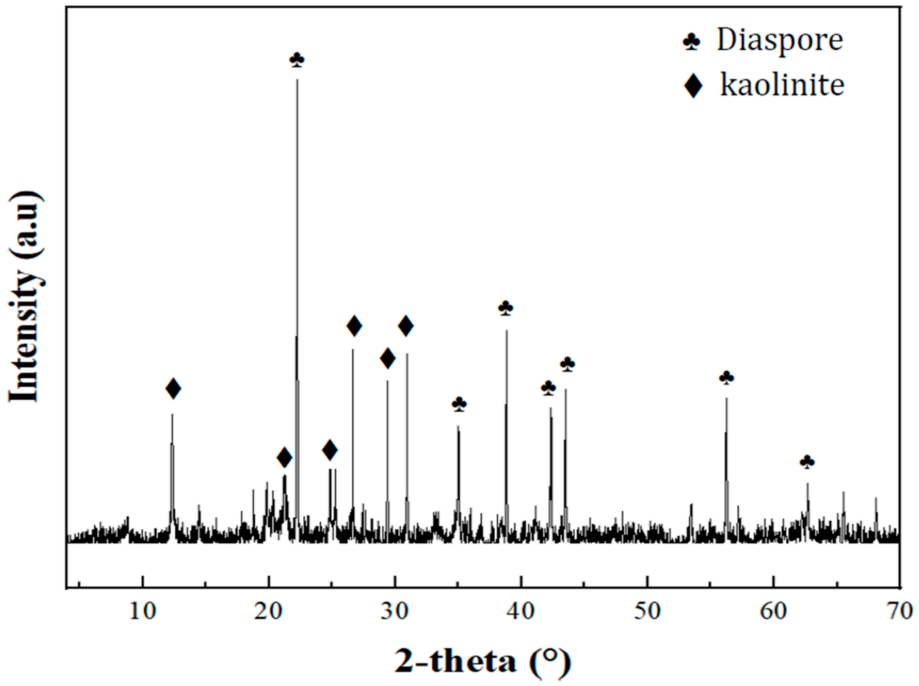


Figure 2. Bauxite mineral sample X-ray diffraction pattern.

The main recognized phases are diaspore (AlO(OH)) and kaolinite ($Al_2Si_2O_5(OH)_4$). Diaspore has multiple sharp diffraction peaks, with the highest peak at 2θ = 22.5°, which confirms its elevated concentration in the sample. The finding of several diffraction peaks corresponding to diaspore in the 20–60° range further confirms that it is the main crystalline aluminum mineral phase, consistence with the high Al_2O_3 concentration reported by XRF.

The distinctive reflections of kaolinite, especially those between 12° and 30° 2θ, are clearly detected, albeit at reduced strength. The peaks are revealed to be well-ordered kaolinite layers and are consistent with the relatively high SiO_2 concentration obtained by XRF. This demonstrates that kaolinite is a secondary but important part of the bauxite matrix. No reflections could be assigned to gibbsite, boehmite or quartz, indicating their absence or concentrations below the detection limit. The XRF characterization indicated

relatively significant Fe_2O_3 and noticeable TiO_2 contents but no distinguishable diffraction peaks for crystalline iron- or titanium-bearing minerals (goethite, hematite or anatase) were detected. This apparent disparity is probably attributed to Fe and Ti being present in weakly crystalline, amorphous or finely dispersed phases, giving weak diffraction signals or being obscured by the apparent reflections of the kaolinite and diaspore.

The predominant crystalline phase is determined to be diaspore. This is in agreement with the XRF data showing the Al_2O_3-rich composition, which is a typical composition of diasporic bauxite. It is of great interest for both alumina production and environmental geochemistry research due to its high aluminum content and stability in certain geochemical environments.

The combined XRF, XRD, FTIR and SEM-EDS characterizations provide complementary information to assess the mineralogical controls on heavy metal retention and release during leaching. Structural and surface-mediated interactions of heavy metals with diaspore and kaolinite as a function of pH and sulphate changes are explored. The Shanxi bauxite is defined by a combined interpretation of XRF, XRD, FTIR and SEM–EDS studies, and it is an Al-rich and Fe-bearing aluminosilicate with crystalline diaspore and kaolinite, and accessory Fe- and Ti-bearing phases.

3.1.3. Surface Morphology and Related Minerals

The microstructural properties and elemental distribution of the bauxite sample were investigated by SEM with EDS.

The SEM micrograph (Figure 3a) demonstrates a heterogeneous microstructure (a volume of ore around 70 cubic microns) consisting of aggregated mineral grains with irregular forms and a different contrast that indicates differences in phase composition and density. The EDS spectrum (Figure 3b) reveals the presence of significant elements such as Al, O, Fe, Si and Ti, and trace quantities of environmentally relevant metals such as As, Cd, Cr, Cu, Ni, Pb and Zn. The quantitative analysis demonstrated that aluminum and oxygen were the most abundant elements in the matrix, which is compatible with the prior identification of the existence of the bauxite mineral framework by XRD and FTIR.

Elemental mapping reveals a complicated trace metal distribution. The distribution of aluminum is homogeneous, but Fe, Ti and Mn are localized in certain locations indicative of the presence of small oxides or related phases. Arsenic, lead and chromium have scattered but concentrated patterns, assumed to be adsorbed on iron- or aluminum-rich sites. Other metals such as Cd, Cu and Zn are more diffuse and are likely to be due to non-specific sorption on a variety of mineral surfaces.

These experimental results demonstrated the capacity of the bauxite matrix to retain many minerals, where aluminum oxides, iron oxides and clays act synergistically to immobilize the heavy metals. The irregular distribution of certain elements, especially As, Cr and Pb, suggests that their mobility may be important in acidic or reducing environments, especially when their host phases are destabilized.

The SEM–EDS elemental maps demonstrate a widespread presence of Fe and a more limited distribution of Ti in the bauxite matrix, besides the predominant diaspore and kaolinite phases. These observations reveal the existence of supplementary Fe- and Ti-bearing mineral phases, compatible with the mineralogical composition determined by XRD. Although the crystallographic character of these phases cannot be identified univocally by SEM-EDS and FTIR, they provide complementary evidence of their geographical distribution. These Fe- and Ti-bearing phases can also play a role in heavy metal retention through adsorption and surface complexation processes, and thus impact the geochemical behavior of trace elements during AMD leaching.

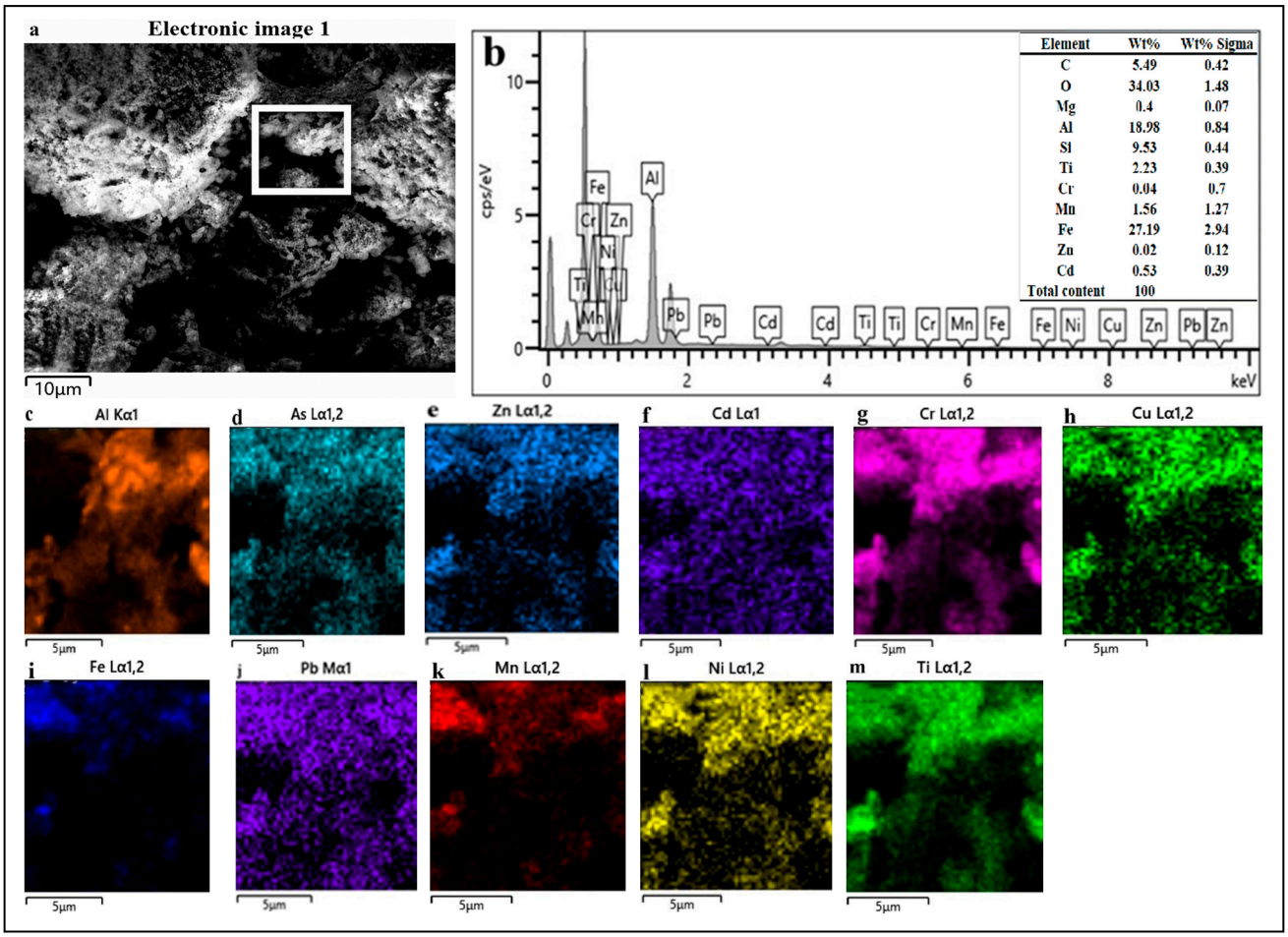


Figure 3. Energy spectrum of sample bauxite ore. (**a**) Environmental scanning electron microscope backscattering image; (**b**) energy spectrum analysis spectrum at the white box in Figure (**a**); surface scan distribution characteristics of metals in the white box in Figure (**a**): (**c**) Al; (**d**) As; (**e**) Zn; (**f**) Cd; (**g**) Cr; (**h**) Cu; (**i**) Fe; (**j**) Pb; (**k**) Mn; (**l**) Ni; (**m**) Ti.

In brief, the SEM-EDS analysis supports the results of the XRD and FTIR by verifying the mineralogical heterogeneity and explaining the spatial correlations between the host phases and the trace metals. Micro- to nano-scale associations are essential for understanding the leaching potential and environmental behavior of heavy metals in bauxite under mine water conditions.

XRF characterization indicated a relatively large Fe_2O_3 content; however, XRD did not identify apparent diffraction peaks attributable to crystalline iron oxides. Such apparent disparity is most likely due to Fe being present in weakly crystalline, finely distributed or amorphous phases, whose weak diffraction signals are obscured by the dominating peaks of diaspore and kaolinite. This conclusion is corroborated by the elemental maps from SEM-EDS, which reveal that Fe is widely distributed throughout the bauxite matrix. Thus, the combined XRF, XRD, and SEM-EDS investigations provide complementary evidence of the occurrence of Fe-bearing phases in the examined bauxite.

3.1.4. Functional Group Analysis by FTIR Spectroscopy

In order to identify the primary functional groups associated with mineral phases in the bauxite sample, FTIR spectroscopy was implemented. The FTIR spectrum (Figure 4) presents many well resolved absorption bands, which are useful for the XRF and XRD investigation pointing out the existence of hydroxylated and silicate structures within bauxite matrix.

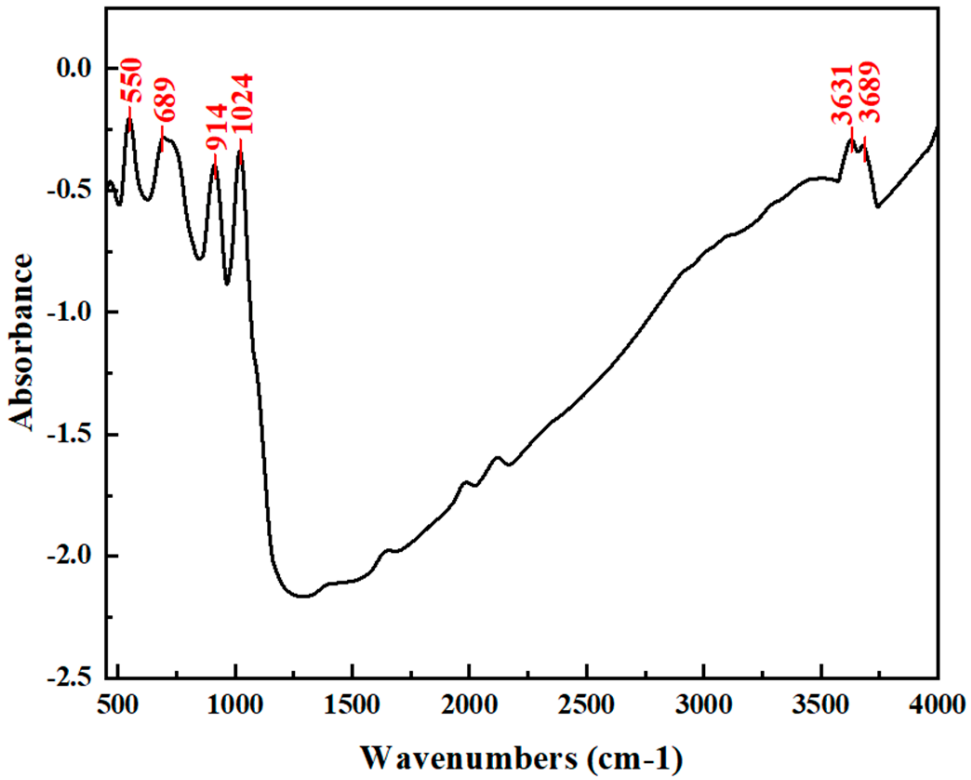


Figure 4. FTIR spectrum of bauxite ore sample.

The wide and strong bands at 3689 cm^{-1} and 3631 cm^{-1} for Al-bearing minerals (diaspore and kaolinite) are related to O-H stretching vibrations of structural hydroxyl groups. These bands are characteristic of inner surface hydroxyls engaged in hydrogen bonding in stratified or hydroxide-type structures. The absorption peak of the bands at 1024 cm^{-1}, attributed to Si-O stretching vibrations, is consistent with the presence of phyllosilicates, especially kaolinite, and supports the XRD identification of this mineral, as well the relatively high SiO_2 content determined by XRF. The band at 914 cm^{-1} is assigned to Al-OH bending vibrations, which are characteristic of octahedrally coordinated aluminum in kaolinite and diaspore. The bands detected around 689 cm^{-1} and 549 cm^{-1} are predominantly assigned to the Al-O-H and Al-O bending vibrations of diaspore and kaolinite. These bands may comprise minor contributions from Fe-O and Ti-O vibrations related to accessory Fe- and Ti-bearing phases, given the relatively high Fe_2O_3 and detectable Ti_2O_3 contents as measured by XRF, together with the SEM-EDS elemental maps showing a widespread distribution of Fe and a localized presence of Ti.

Overall, the FTIR spectrum is consistent with the presence of hydroxylated aluminum minerals and silicate clays, in agreement with the identification of the bauxite mineral framework as reported by XRD, and the Al_2O_3- and SiO_2-rich chemical composition determined by XRF. Moreover, the prevalence of structural hydroxyl groups in the O-H stretching region may suggest the availability of reactive surface sites contributing to surface complexation and metal adsorption. Surface functional groups are anticipated to play a role in limiting retention and the release of heavy metals in leaching under varied geochemical conditions.

3.1.5. Minerals Controlling Metal Mobility and Retention

Mineralogical composition of bauxite is a regulating factor for retention and mobility of heavy metals in bauxite. Particular mineral phases have specific roles according to their surface chemistry, structural characteristics and stability in acid or sulphate condition.

The behavior of heavy metals in bauxite systems is determined by the characteristics and amounts of component minerals, which act as sinks or sources according to their surface reactivity and environmental stability. The combined XRF, XRD and FTIR analyses show that the bauxite is an Al-rich, Fe-bearing aluminosilicate ore, dominated by diaspore (AlO(OH)) and kaolinite ($Al_2Si_2O_5(OH)_4$), providing a mineralogical and geochemical basis for the interpretation of heavy-metal immobilization under acidic, sulfate-rich leaching conditions.

The main phase, diaspore, comprises many structural hydroxyl groups that may form surface complexes with divalent and trivalent ions such as Pb^{2+}, Cu^{2+}, Zn^{2+}, and Cr^{3+}. Strong adsorption of trace metals to the surface, especially in neutral-to-moderately acidic conditions, leads to high surface activity. Under severely acidic conditions (pH < 4) the solubility of diaspore is increased and metals previously adsorbed or incorporated in the structure may be released. This result correlates well with the high Al_2O_3 content obtained by XRF.

The layered aluminosilicate mineral kaolinite contains trace metals. The material has flat and edge surfaces for ion exchange and weak surface complexation with metal species. Kaolinite buffers and immobilizes metal in low-Fe mineral matrices, but its retention capacity is less than that of Fe- and Al-oxides. Metal retention by kaolinite may be lost under acidic and competitive anionic environments such as sulphate, resulting in accelerated metal desorption. Although no distinct diffraction peaks attributable to crystalline Fe-bearing minerals were observed by XRD, the relatively high Fe_2O_3 content determined by XRF and the widespread Fe distribution revealed by SEM–EDS strongly suggest the occurrence of poorly crystalline or finely dispersed iron-bearing phases. These phases are well known for their high affinity toward oxyanions and divalent metals through surface complexation and co-precipitation processes. These minerals have a high sorption capacity and affinity for metals that are sensitive to redox conditions such as arsenic and chromium in inner-sphere complexes. In reduction or acidic conditions, dissolution can shift them from immobilizing to releasing contaminants. Similarly, the TiO_2 content measured by XRF, together with the localized Ti distribution observed by SEM–EDS, suggests the presence of accessory Ti-bearing minerals that may provide a limited contribution to metal adsorption because of their comparatively low surface reactivity. Quartz (SiO_2) is inert and has no functional adsorption sites and so does not hold metal.

The combined chemical (XRF) and mineralogical (XRD, FTIR and SEM–EDS) characterization demonstrates that the investigated bauxite is dominated by diaspore and kaolinite, together with accessory Fe- and Ti-bearing phases, which collectively influence the retention and release of heavy metals during interaction with acid mine drainage. The geochemical behavior of trace elements is therefore governed by the dissolution–precipitation reactions of these mineral phases, the availability of reactive surface hydroxyl groups, and the abundance of Fe-bearing phases, with pH and sulfate concentration acting as the principal environmental controlling factors.

3.2. Leaching Behavior of Heavy Metals

3.2.1. Acid-Soluble Heavy Metals in Bauxite

The heavy metals (As, Cd, Cr, Cu, Ni, Pb and Zn) in the raw bauxite samples were determined by acid digestion and ICP-OES analysis. To consider the effect of particle size, the materials were divided into several size fractions (<0.1 mm, 0.1–0.3 mm, 0.9–1.3 mm, 1.3–1.43 mm and total fraction <1.43 mm) and each fraction was analyzed in quintuplicate (n = 5). The results are given in Table 2.

Table 2. Acid-soluble heavy metal concentrations.

Particles	As (mg/kg)	Cd (mg/kg)	Cr (mg/kg)	Cu (mg/kg)	Pb (mg/kg)	Ni (mg/kg)	Zn (mg/kg)
<0.1 (mm)	0.151	0.004	0.031	0.069	0.079	0.348	2.094
0.1–0.3 (mm)	0.106	0.001	0.021	0.054	0.015	0.179	0.480
1.3–0.9 (mm)	0.112	0.002	0.025	0.051	0.026	0.160	0.155
0.9–1.43 (mm)	0.119	0.006	0.027	0.054	0.138	0.143	0.076
<1.43 (mm)	0.105	0.006	0.024	0.048	0.130	0.118	0.040
Mean	0.118	0.004	0.025	0.055	0.078	0.190	0.569
Minimum	0.105	0.001	0.021	0.048	0.015	0.118	0.040
Maximum	0.151	0.006	0.031	0.069	0.138	0.348	2.094
Standard Deviation	0.019	0.002	0.003	0.008	0.057	0.092	0.870

These data allow for the evaluation of metal release during leaching experiments and the determination of leaching efficiency based on the acid-soluble metal content of the solid phase.

3.2.2. Effect of $Ca(OH)_2$ on Heavy Metals Removal

The removal efficiencies of heavy metals (As, Cd, Cu, Cr, Ni, Pb and Zn) were affected by $Ca(OH)_2$ treatments, and metal-specific trends were found under acid-sulphate leaching conditions. The baseline (simulated mine water) was of pH = 3, with $Ca(OH)_2$ values of 0.014–0.14 mol/L.

Figure 5 demonstrates the heavy metal removal efficiency variation with the dosage of $Ca(OH)_2$. In general, most metals perform efficiently at alkaline conditions; however, the behavior is element-specific and not always linear. As, Pb and Zn showed relatively high and constant removal efficiencies, often between 90 and 100%, indicating effective immobilization through precipitation and adsorption. Cd is almost completely removed in most treatments, whereas Ni is high and rather constant (>90%).

The efficiency of Pb removal rapidly rose from around 11% in the untreated acidic environment to almost complete removal after addition of $Ca(OH)_2$. After then, the removal efficacy was about 100% in the other treatment settings, which means that the immobilization of Pb was stable when the conditions were sufficiently alkaline. This behavior is consistent with the low solubility of Pb hydroxide and increased adsorption of Pb on newly generated hydroxide precipitates and mineral surfaces.

Cu exhibits moderate-to-high efficiency, with values ranging from about 70% to 100%, suggesting sensitivity to the geochemical parameters of the system. Cr displays an increasing elimination (≈70%–90%) with the increase in $Ca(OH)_2$ dosage, consistent with progressive hydroxides precipitation under alkaline conditions.

For several elements the measured values around or similar to 100% indicate a substantial immobilization of metals under alkaline conditions. In summary, the enhancement of heavy metal immobilization is noticed with the rise in $Ca(OH)_2$ dosage with the stabilization of efficiencies under conditions from near neutral to alkaline with the dominance of precipitation and adsorption mechanisms.

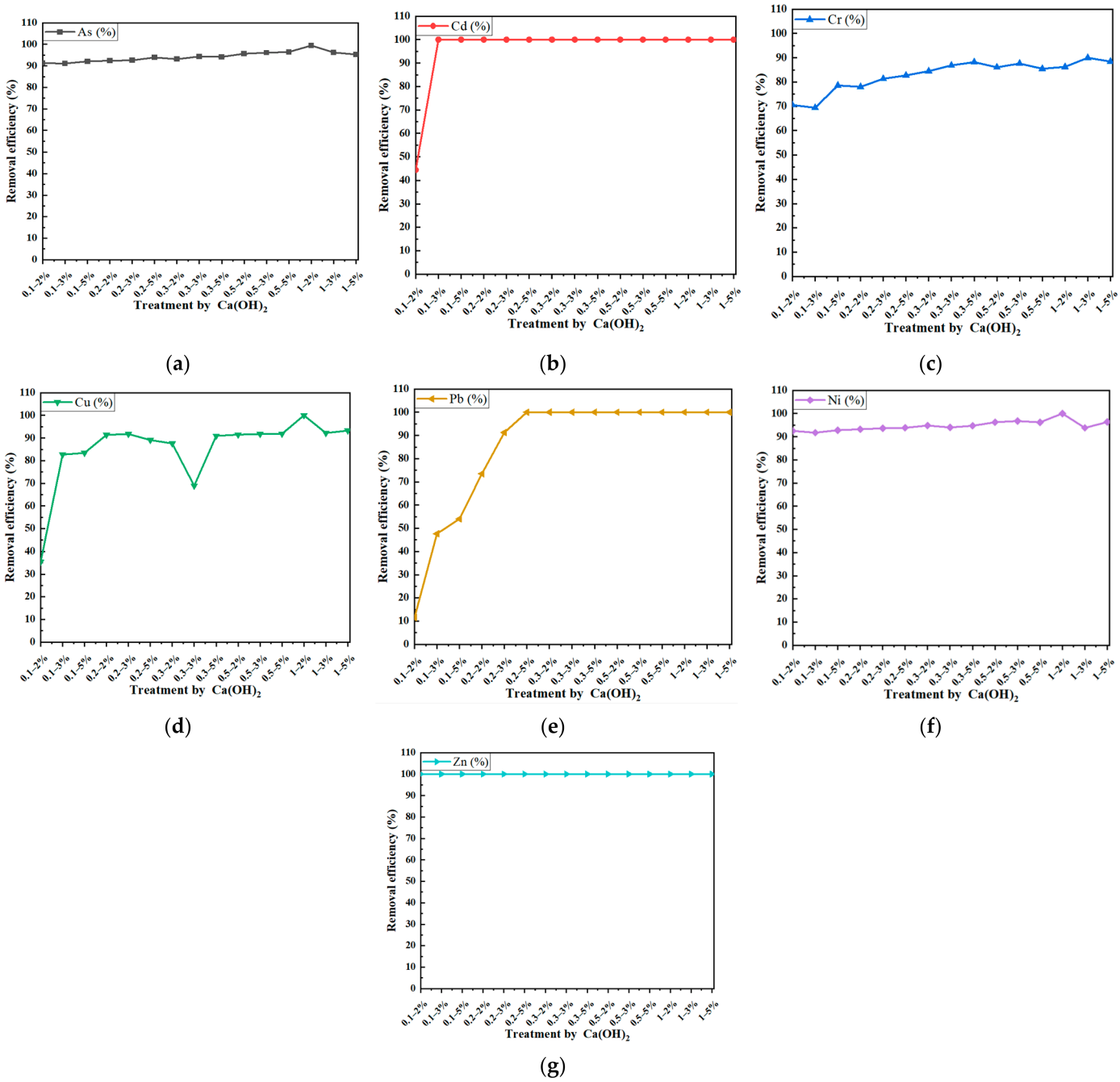


Figure 5. Removal efficiency of heavy metals with Ca $(OH)_2$ treatment, such as: (**a**) removal efficiency of As; (**b**) removal efficiency of Cd; (**c**) removal efficiency of Cr; (**d**) removal efficiency of Cu; (**e**) removal efficiency of Pb; (**f**) removal efficiency of Ni; (**g**) removal efficiency of Zn.

The nearly 100% removal efficiency should be examined with appropriate sensitivity in the context of the analytical uncertainty, especially when residual dissolved metal concentrations are close to the ICP-OES detection limit. Small analytical differences at very low concentrations can lead to apparent removal efficiencies close to or equal to 100%. Thus, these figures should be considered as an indication of near-complete immobilization of dissolved metals under the studied experimental conditions rather than an absolute removal. The gradual increase in pH coupled with the considerable diminution in dissolved metal concentrations is consistent with the prediction that hydroxide precipitation, adsorption and surface complexation were the primary processes influencing metal immobilization.

3.2.3. Effect pH and Sulphate Concentration

The regulation of metal release was significantly influenced by pH, thereby confirming that pH is the major factor determining the immobilization mechanisms in the system examined. Increasing the pH from acidic (3) to alkaline conditions significantly improved the removal efficiency of As, Cd, Pb, and Zn. The change from acidic conditions to near neutral and alkaline pH (7.4–11.0) promoted the reduction in dissolved quantities of As, Cd, Cr, Cu, Ni, Pb and Zn (Figure 6). This progression reflects the gradual formation of thermodynamically favorable conditions for precipitation of metal hydroxides and adsorption on aluminosilicate and oxyhydroxide surfaces.

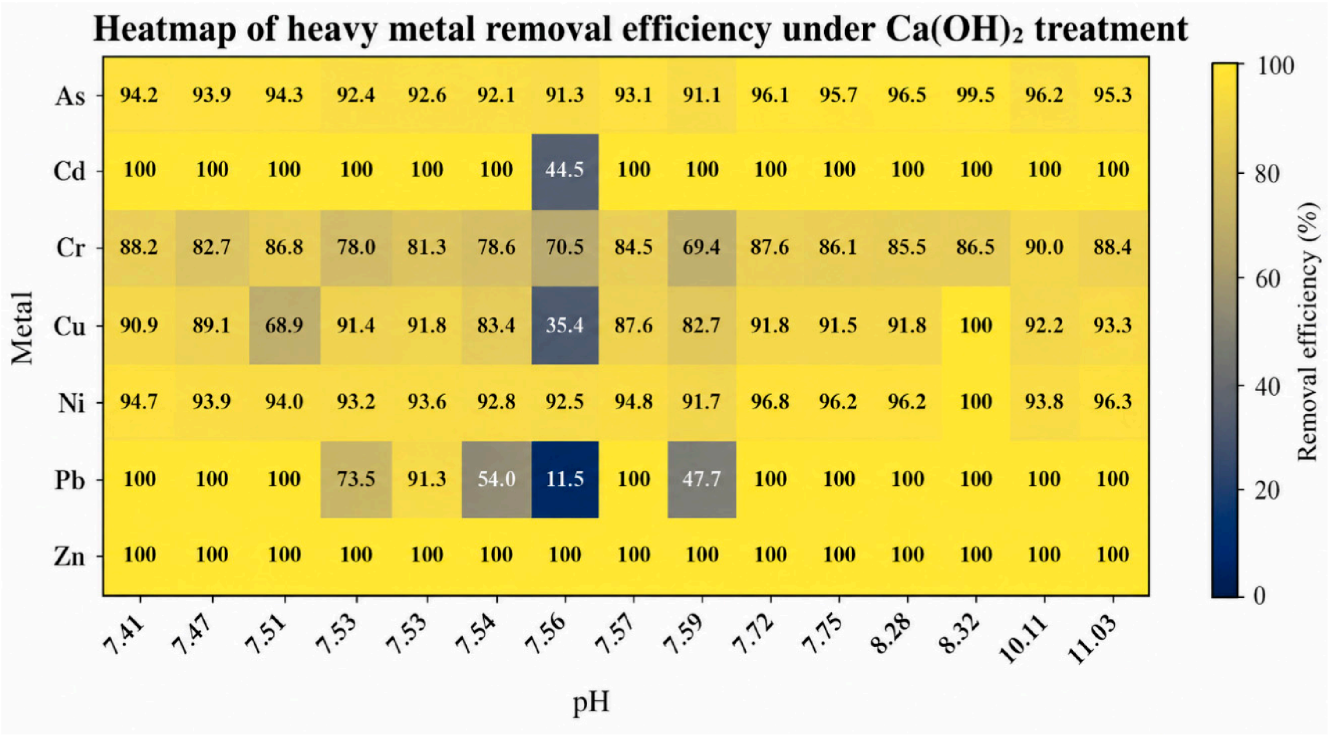


Figure 6. Heatmap of the removal efficiency (%) of heavy metals as a function of the final pH after $Ca(OH)_2$ treatment. Values are measured removal efficiency. High removal efficiency is shown by light-yellow colors whereas lower removal efficiencies are indicated by dark-blue colors.

The high efficiencies obtained for Pb, Zn and Cd reveal that these metals rapidly become unstable in solution with increasing pH, favoring the precipitation of poorly soluble phases such as $Pb(OH)_2$, $Cd(OH)_2$, and $Zn(OH)_2$. The increasing rise in Cr removal efficiency with pH also shows a conversion to less mobile trivalent species related to the precipitation of $Cr(OH)_3$ at alkaline conditions.

The relative stability of As (>90%) suggests that arsenate species have a high attraction for Al- and Fe-rich surfaces, where surface complexation and co-precipitation mechanisms dominate at high pH. Cu and Ni demonstrate a more moderate variability, which may be due to a greater sensitivity to speciation equilibria, competition for adsorption sites and ionic interactions in solution.

Sulphate, held constant at an initial concentration in this work, does not appear to be the regulating factor for metal mobility, but it does contribute indirectly to the geochemical stability of the system by raising the ionic strength and the likely production of secondary sulphate phases. Thus, the results suggest that the immobilization of metals under the simulated AMD conditions is mainly dominated by alkaline precipitation mechanisms and surface adsorption due to the increase in pH.

Based on this profile (Figure 7), the range between pH~7.5 and 12 (dosages $\geq$ 2%) promotes hydroxide precipitation and co-precipitation with sulphates, maximizing metal retention. Very high pH (>11) can lead to the re-dissolution of certain amphoteric metals (for example, Zn) under real-world conditions, so fine-tuning treatment dosage is important.

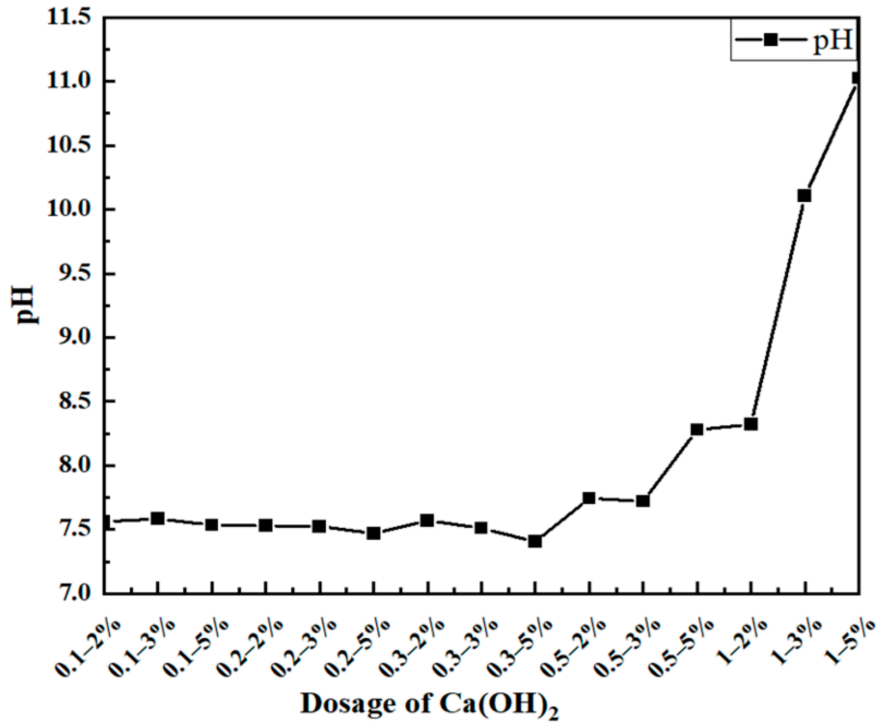


Figure 7. Evolution of pH as a function of the dosage of $Ca(OH)_2$.

3.2.4. Temporal Evolution of Metal Release

The studies were carried out in batch equilibrium settings but the changes seen with the dosage of $Ca(OH)_2$ show a progressive evolution of the geochemical mechanisms governing the immobilization of metals. Low dosages of $Ca(OH)_2$ correlate to conditions where neutralization is partial, which restricts the production of poorly soluble metallic phases and keeps a larger fraction of metals in dissolved form. This is especially evident for Cu, Cr and Pb, whose removal efficiencies remain rather low at the lowest dosages.

The progressive removal efficiencies with the increase in $Ca(OH)_2$ dosage indicate that the increase in pH pushes the speciation equilibria towards more thermodynamically stable forms. This evolution favors the precipitation of metal-hydroxides, adsorption on aluminosilicate surfaces and co-precipitation with secondary phases generated during neutralization. The results indicate that As, Cd, Ni and Zn rapidly attain significant immobilization levels (>90%) suggesting that their mobility is strongly restricted as soon as conditions approaching neutrality are introduced.

The progressive increase in Cr and Pb removal efficiency shows a stronger dependence on the alkalinization of the medium, suggesting that their immobilization is mainly regulated by the production of weakly soluble hydroxylated phases. The behavior of Cu with a remarkable enhancement of immobilization with rising pH further supports the significance of precipitation and adsorption mechanisms in diminishing its mobility.

The results indicate that metal retention in acid-mine-water-impacted systems is not instantaneous, but the outcome of a protracted geochemical evolution characterized by pH increase and stabilization of secondary mineral phases. Such interpretation verifies alkaline neutralization as the primary mechanism governing metal mobility and is a critical process in designing passive treatment solutions for AMD.

3.2.5. Variations in Metals Depending on the Host Mineral Phases

The variations discovered between the metals indicate different immobilization mechanisms governed by their geochemical speciation and their interaction with the mineral phases of bauxites. As removal efficiency was >90%, demonstrating a strong affinity between As and Al and Fe-rich surfaces, where unique adsorption mechanisms become dominant in alkaline conditions.

Cd and Zn obtained efficiencies close to 100%, revealing that their mobility is substantially constrained by the precipitation of metal hydroxides when pH increases. Likewise, the progressive enhancement in Cr removal efficiency from 70% to nearly 90% supports the fact that its retention is mainly controlled by the formation of poorly soluble hydroxylated phases.

Cu displays a considerable increase in the removal efficiency with the increase in $Ca(OH)_2$ dose, indicating that its immobilization is more dependent on the alkalinization of the medium and the subsequent development of adsorption and precipitation mechanisms. The most sensitive dependence on pH is revealed by Pb with efficiencies varying from low beginning values to almost complete immobilization, confirming the prominent function of the precipitation of weakly soluble lead phases.

Ni exhibits excellent removal efficiency (>90%) in all treatments, implying immobilization through surface adsorption and partial precipitation under alkaline environment. These results suggest that the differences found between the metals are mostly controlled by their geochemical behavior in response to the increase in pH rather than by the mineralogical composition of the bauxite alone.

4. Discussion

4.1. Correlation Between Mineralogy and Metal Mobility

The mineralogical characterization of bauxite, which is dominated by diaspore (AlO(OH)) and kaolinite ($Al_2Si_2O_5(OH)_4$), gives vital information on the geochemical mechanisms governing the mobility of heavy metals under simulated AMD conditions. Information about the main mineral phases and functional groups of bauxite was obtained via XRD and FTIR analyses, whereas trace elements were not measured directly. However, these findings give a crucial basis for the interpretation of the adsorption, dissolution–precipitation and surface complexation mechanisms that control the behavior of heavy metals.

The predominant aluminum oxyhydroxide phase, diaspore, shows a strong surface reactivity owing to the presence of hydroxyl groups (≡Al–OH). The increase in pH generated by the addition of $Ca(OH)_2$ facilitates the deprotonation of these groups and increases the number of reactive sites accessible for the adsorption of dissolved molecules. This result is in accordance with the high removal efficiencies exhibited for As (91.09%–99.45%), suggesting that aluminum-rich surfaces play a significant role in the retention of oxyanions through surface complexation [52]. The presence of Ca^{2+} can also facilitate the binding of metals through electrostatic bridging mechanisms between mineral surfaces and dissolved species [53]. Thus, the higher immobilization at higher pH is thermodynamically linked to lower metal solubility and increased surface affinity of Al-rich mineral phases.

Kaolinite also assists in the fixation of metals by surface adsorption and complexation processes at its reactive sites. The high efficiencies found for Ni (91.72%–100%), Cd (44.50%–100%) and Zn (100%) show that the increase in pH enhances simultaneously the attachment on mineral surfaces and the precipitation of metal hydroxides. On the other hand, protonation of mineral surfaces under acidic circumstances limits the availability of adsorption sites and enhances the mobility of dissolved metals [54,55].

The experimental results reveal that the steady rise in $Ca(OH)_2$ dose is conducive to the immobilization of metals. This trend is more marked for Pb, whose removal effectiveness

goes from 11.50% to 100%, for Cu from 35.41% to 100%, and for Cr from 70.55% to over 90%. These trends suggest that the precipitation of metal hydroxides is the dominant process controlling metal mobility. The corresponding precipitation reactions are presented in Section 4.2 (Equations (2)–(4)).

Although sulphate ions might contribute to the secondary mineral phase development, such as $PbSO_4$, their geochemical influence was secondary in the present investigation, as sulphate concentrations were kept constant throughout the experiments [56]. Thus, pH-dependent precipitation and adsorption processes were the main mechanisms driving trace metal immobilization.

The results reveal consistent and physically plausible patterns, demonstrating the almost total immobilization of Cd, Pb and Zn under the most alkaline conditions.

In general, the results indicate that the mineralogical composition provides reactive surfaces that favor metal fixation, while pH is the main geochemical parameter that controls metal mobility and stabilization in bauxite systems impacted by AMD [57]. Aluminum-rich mineral assemblages favor adsorption and precipitation processes in alkaline circumstances, while their retention capability is dramatically reduced in acidic conditions. These data confirm that alkaline amendment is an efficient strategy to reduce the mobility of heavy metals, while stressing the importance of local mineralogical and geochemical variables in the efficiency of remediation strategies.

4.2. Geochemical Processes Controlling Metal Release

The release and mobilization of heavy metals under simulated acid sulphate mining drainage conditions are controlled by pH-dependent geochemical processes such as dissolution, precipitation, surface complexation and ion exchange, and not just by the mineralogical presence of trace elements. Experimental results show that pH is the key governing factor of metal mobility, whereas sulphate content and mineral composition have a secondary influence on the behavior of As, Cd, Cr, Cu, Ni, Pb and Zn.

Under acidic conditions, the high activity of H^+ ions promotes the dissolution of mineral surfaces and the concentration of dissolved metal species. At the same time, protonation of surface functional groups decreases the number of reactive sites for adsorption, hence enhancing the mobility of metals in solution. In such settings, Cu, Zn and Ni are largely in a soluble ionic state, which facilitates transport and bioavailability.

The steady increase in pH due to the addition of $Ca(OH)_2$ tends to move the system towards conditions conducive for precipitation of metal hydroxides and adsorption on mineral surfaces. The increase in removal efficiencies of Pb, Cu and Cr is directly consistent with this development. The almost total immobilization of Cd and Zn and the significant retention of As and Ni indicate that hydroxide precipitation and surface complexation are the predominant retention processes [58,59], such as:

$$Pb^{2+} + 2OH^- \rightarrow Pb(OH)_2 \quad (2)$$

$$Zn^{2+} + 2OH^- \rightarrow Zn(OH)_2 \quad (3)$$

$$Cr^{3+} + 3OH^- \rightarrow Cr(OH)_3 \quad (4)$$

The increase in pH also encourages the deprotonation of aluminosilicate and oxyhydroxide surfaces, thus increasing the density of sorption sites and improving the retention of dissolved metals. High efficiencies found for As (91%–99%) especially imply excellent adsorption on surfaces rich in aluminum and iron.

Sulphate ions can alter the ionic strength of the system and participate in the creation of secondary sulfate phases. However, their action was limited in the present investigation as their initial concentration was constant throughout all the tests [60]. Therefore, the

fluctuations of metal mobility observed are mainly ascribed to the changes in speciation and precipitation equilibria generated by pH.

The partial dissolution of aluminosilicate phases and aluminum oxyhydroxides also releases Al^{3+} ions, which are believed to be involved in co-precipitation processes and in the production of secondary phases contributing to the immobilization of metals [61]. Thus, the neutralization of acid mine fluids proceeds with simultaneous dissolution and secondary mineral precipitation processes.

XRD and FTIR analyses were used to identify primary mineral phases and functional groups involved in metal retention, but were not directly able to detect trace elements. The abundance of diaspore and kaolinite provides reactive surfaces amenable to adsorption and precipitation mechanisms. Moreover, iron oxyhydroxides like ferrihydrite and goethite have highly reactive hydroxyl sites that can easily adsorb arsenic and chromium molecules [62].

High arsenic removal efficiencies demonstrate considerable affinity of As(V) for Fe and Al-rich surfaces via inner-sphere complexation:

$$\equiv FeOH + H_2AsO_4^- \rightarrow \equiv FeH\ AsO_4^- + H_2O \quad (5)$$

Similarly, the steady increase in Cr removal efficiency with increasing pH suggests enhanced Cr immobilization, likely resulting from $Cr(OH)_3$ precipitation and reduced mobility of Cr under alkaline conditions [63].

The calculated and experimental results reveal a good agreement. In summary, the results indicate that the primary mechanisms for immobilization of heavy metals in bauxite systems influenced by AMD are precipitation of metal hydroxides and pH-controlled surface complexation. The main purpose of mineralogy is to offer the reactive surfaces for these reactions to occur and the alkalinity limits the efficacy of these processes. These results confirm that regulated pH adjustment is an efficient geochemical method to minimize the mobility of heavy metals and the environmental concerns in bauxite environments affected by AMD [64]. However, further investigation should involve the quantitative thermodynamic interpretation through PHREEQC to speciation models and saturation indices and secondary mineral stability.

4.3. Environmental Implications Under AMD

AMD is a significant cause of environmental contamination as it can mobilize heavy metals and transport them to surface and groundwater. The data obtained reveals that the leaching of trace elements present in bauxite is favored under acidic conditions, confirming the risk of metal dispersion in mining areas exposed to acid sulfate waters.

The remarkable increase following alkaline neutralization confirms the dominant role of pH in regulating heavy metals transport. These studies demonstrated that alkaline conditions favor the immobilization of metals by precipitation and adsorption, therefore limiting their availability for hydrogeochemical transport and bioaccumulation in aquatic ecosystems [40,65]. Conversely, under acidic conditions they are likely to remain in solution and are more apt to contaminate sediments, aquatic creatures and water resources [41,49].

The efficiency of the $Ca(OH)_2$ therapy observed indicates that alkaline neutralization is an efficient strategy for reducing metal mobility in systems affected by AMD [65–67]. Results reveal that the mobility of metals is mostly controlled by pH, while the mineralogy of bauxite has a major influence on the availability of reactive surfaces for adsorption and precipitation processes.

These observations underline the need to include mineralogical and geochemical characterization in the environmental monitoring programs of bauxite sites. The integration of laboratory experimental results and hydrogeochemical modeling methodologies at the

field scale would improve the prediction of heavy metal behavior and the effectiveness of long-term remediation initiatives.

4.4. Comparison with Literature and Similar Studies

The leaching behavior documented in this work is in agreement with the mechanisms reported for mining wastes, aluminosilicate minerals and systems affected by AMD, as revealed in Table 3.

The high removal efficiencies achieved for As, Pb, and Cd are in line with the increase in pH promoting the precipitation of metal hydroxides and the co-precipitation mechanisms as described by Herath et al. (2023) [68] and Tian et al. (2024) [69]. These data indicate that alkalinization is the key factor controlling metal retention in AMD-contaminated systems.

The gradual increase in Cr and Cu removal efficiencies with the increase in $Ca(OH)_2$ dosage further confirms the predominant role of precipitation and adsorption processes under alkaline circumstances. This progression is consistent with the observations of Equeenuddin et al. (2013) [70] and Lottermoser (2010) [41] who suggested that the mobility of metals improves dramatically under acidic conditions due to the dissolution of carrier phases and decrease in adsorption capabilities..

The high efficiencies measured for Ni and Zn show that their mobility declines rapidly as soon as near-neutral conditions are achieved. These results support the conclusions of Alankangas et al. (2013) [71], according to which alkaline neutralization is the most effective strategy to restrict the transfer of metals in mining environments.

The results also point to the importance of mineralogy in creating reactive surfaces that are favorable for adsorption and co-precipitation. This result is compatible with the work of (Lweya et al., 2015) [72] that revealed the implication of Fe and Al-rich phases in Cu retention, and also with the study of Gonçalves et al. (2024) [73] about the efficiency of bauxite-derived materials for the treatment of acid mine fluids. Similarly, Babel and Kurniawan (2003) [74] highlighted the ability of aluminosilicate materials to immobilize heavy metals through adsorption.

This current study presents a mechanistic evaluation of heavy metals in bauxite under simulated AMD settings. Nevertheless, there are several limitations related to this study. The results of the experiment strongly indicated the development of secondary metal-carrying precipitates during $Ca(OH)_2$ neutralization. The solid phases, however, were not directly characterized in the present work. The observed increase in pH and the considerable decrease in dissolved metal concentrations indicate that the precipitates are likely to comprise metal hydroxides, mixed hydroxide phases and possibly metal-bearing sulphate minerals.

In addition, the long-term environmental stability of these precipitates can depend on future geochemical conditions. Further drops in pH induced by recurrent AMD development, seasonal hydrological changes or climatic variations may result in partial dissolution of some secondary phases and favor remobilization of metals previously immobilized. Therefore, the immobilization reported in this study has to be considered conditional to the maintenance of favorable alkaline conditions.

Table 3. Heavy metal removal efficiency treatment in similar studies.

Metals	Matrix	Treatment/Condition	Findings	Study
Multiple metals (AMD context)	Mine wastes water	Natural AMD	Metal release strongly pH-dependent; mineral buffering governs mobility	Lottermoser (2010) [41]
Fe, Cu, Zn, and other trace metal	Sulfidic mine wastes + alkaline by-products	Neutralization mixes	Neutralization prevented AMD formation, reduced metal release	Alankangas et al. (2013) [71]
Pb, Cd, Cr, Ni, Cu, Zn	Aqueous solutions	Low-cost adsorbents (natural and waste-derived)	Adsorption effective in removing metals; mineral surfaces play key role	Babel and Kurniawan (2003) [74]
Fe, Cd, Al, trace metals	AMD sediments	pH variation	pH controlled precipitation/adsorption of metals; similar mechanism to bauxite leaching	Equeenuddin et al. (2013) [70]
Cu	Lateritic soils, groundwater	Natural leaching and transport	Cu mobility regulated by laterite mineralogy and pH	Lweya et al. (2015) [72]
Cd	Soil with bauxite residue	Water management + residue application.	Cd immobilization via sorption and precipitation	Tian et al. (2024) [69]
Pb, Cd, Ni, Zn	Polluted water	Bauxite sorption experiments	Bauxite effective for heavy metal removal	Herath et al. (2023) [68]
Multi-metals (AMD)	Geopolymer (bauxite-based)	3D-printed treatment blocks	Neutralized AMD and removed multiple metals simultaneously	Gonçalves et al. (2024) [73]
As, Cd, Cr, Cu, Ni, Pb, Zn	Bauxite (diaspore, kaolinite); AMD	Acid sulphate-rich mine water leaching. Ca $(OH)_2$ 2%–5%	Mineralogy (diaspore, kaolinite) controls retention; pH and sulphate regulate dissolution-precipitation. High removal at pH > 7.5	This study

5. Conclusions

The present study investigated the effect of mineral composition on the leaching behavior of heavy metals in Shanxi province bauxite under simulated AMD conditions. In order to isolate the effect of alkaline treatment, the initial pH and sulphate concentration were kept the same in all tests. The combined chemical (XRF) and mineralogical analyses (XRD, FTIR and SEM-EDS) combined with batch leaching tests and chemical analyses helped to identify the major mechanisms controlling the mobility of trace elements.

The results revealed that pH is the main controlling factor of the mobility of heavy metals, while the chemical and mineralogical composition of bauxite determines the availability of reactive surfaces engaged in processes of adsorption, surface complexation and precipitation.

Alkaline neutralization facilitated heavy metal immobilization through the combined effects of metal hydroxide precipitation and interactions with aluminosilicate and Fe-bearing mineral phases as evidenced by the combined XRF, XRD, FTIR and SEM–EDS studies. The results therefore display consistency with the necessity of pH geochemical management in the reduction in the mobility of trace elements in AMD-affected environments.

The combination of bulk chemical composition, mineralogical characterization, and leaching tests in this paper provides new insights into the geochemical mechanisms controlling heavy-metal behavior in bauxite exposed to simulated AMD. However, further research is required to assess the long-term behavior of the metals, to study effects of different sulphate concentrations and different redox conditions, to characterize amorphous ferric phases and the direct identification of metal-bearing minerals using complementary techniques, to characterize the secondary phases generated during neutralization, and to investigate their stability under different environmental conditions.

Author Contributions: Conceptualization, X.F.; methodology, X.F. and S.M.C.; software, S.M.C.; validation, S.M.C. and X.Z.; formal analysis, S.M.C.; investigation, X.F., X.Z. and S.M.C.; resources, X.F.; data curation, S.M.C.; writing—original draft preparation, S.M.C.; writing—review and editing, X.F.; visualization, S.M.C.; supervision, X.F. and X.Z.; project administration, X.F.; funding acquisition, X.F. All authors have read and agreed to the published version of the manuscript.

Funding: The work was funded from National Key R&D Program—Intergovernmental International Science and Technology Innovation Cooperation Special Project (Project No.: SQ2025YFE0106091)—Research on the Air-Space-Ground-Well Monitoring and Early Warning Platform for Water Environment in Deep Mineral Resource Mining Areas.

Data Availability Statement: The original contributions presented in this study are included in the article. Further inquiries can be directed to the corresponding author.

Acknowledgments: Thanks for the great effort by editors and reviewers.

Conflicts of Interest: Xiujuan Feng is employed by Guizhou Rongyuan Environmental Protection Technology Co., Ltd., Guiyang 550081, China. The authors declare no conflicts of interest.

Abbreviations

The following abbreviations are used in this manuscript:

AMD	Acid Mine Drainage
XRD	X-ray diffractometer
FTIR	Infrared spectrometer
SEM-EDS	Scanning electron microscopy and energy dispersive spectroscopy

References

1. Abzalov, M.Z.; Bower, J. Geology of bauxite deposits and their resource estimation practices. *Appl. Earth Sci.* **2014**, *123*, 118–134.
2. Olney, D.; Frisch, N.; Donoghue, A. Bauxite Mining and Alumina Refining: Process Description and Occupational Health Risks. *J. Occup. Environ. Med.* **2014**, *56*, S12–S17. [CrossRef] [PubMed]
3. Zhang, C.; Wang, G.; Zhang, Z.; Zhang, H. Discussion on the Mineralization of Red Soil-Type Bauxite Deposits in the Republic of Guinea. *Chem. Miner. Geol. Resour.* **2015**, *37*, 9.
4. Monsels, D.A.; Van Bergen, M. Bauxite formation on Proterozoic bedrock of Suriname. *J. Geochem. Explor. J. Assoc. Explor. Geochem.* **2017**, *180*, 71–90. [CrossRef]
5. Gao, L.; Wang, D.; Xiong, X.; Yi, C. Summary of the Mineralization Patterns of Aluminum Ore Deposits in China. *Acta Geol. Sin.* **2014**, *88*, 12.
6. Burton, M.; Shegufa, J.Z.; White, B. Public preferences for timeliness and quality of mine site rehabilitation. The case of bauxite mining in Western Australia. *Resour. Policy* **2012**, *37*, 1–9.
7. Konrad, F.; Stalder, R.; Tessadri, R. Quantitative phase analysis of lateritic bauxite with NIR-spectroscopy. *Miner. Eng.* **2015**, *77*, 117–120. [CrossRef]
8. Reddy, M.K.; Ramesh, V.; Kumar, V.S. Mode of Occurrence and Distribution of Bauxite Deposits in Andhra Pradesh and Feasibility of Aluminum Industry. *Procedia Earth Planet. Sci.* **2015**, *11*, 115–121. [CrossRef]
9. Jin, Q. The Current Situation of Bauxite Resources in Henan Province and Suggestions for Sustainable Development. *Fire-Resist. Mater.* **2005**, *39*, 3.
10. Naghadehi, M.Z.; Mikaeil, R.; Ataei, M. The application of fuzzy analytic hierarchy process (FAHP) approach to selection of optimum underground mining method for Jajarm Bauxite Mine, Iran. *Expert Syst. Appl.* **2009**, *36*, 8218–8226. [CrossRef]
11. Gao, Z.; Ke, F.F. Geological characteristics of the red soil type bauxite deposit in Guinea Geological characteristics of the red soil type bauxite deposit in Guinea. *East China Geol.* **2009**, *30*, 115–118.
12. Buchanan, S.; So, H.; Kopittke, P.; Menzies, N. Influence of texture in bauxite residues on void ratio, water holding characteristics, and penetration resistance. *Geoderma* **2010**, *158*, 421–426. [CrossRef]
13. Han, X. *Research on Aluminum Resources and Market Allocation in China*; China University of Geosciences: Beijing, China, 2010.
14. Fu, S. Optimization of bauxite mining process to reduce dilution losses. *Non-Ferr. Met. Des.* **2011**, *38*, 5.
15. Mutakyahwa, M.K.D.; Ikingura, J.R.; Mruma, A.H. Geology and geochemistry of bauxite deposits in Lushoto District, Usambara Mountains, Tanzania. *J. Afr. Earth Sci.* **2003**, *36*, 357–369. [CrossRef]

16. Fontanier, C.C.; Fabri, M.C.; Buscail, R.; Biscara, L.; Koho, K.; Reichart, G.J.; Cossa, D.; Galaup, S.; Chabaud, G.; Pigot, L. Deep-sea foraminifera from the Cassidaigne Canyon (NW Mediterranean): Assessing the environmental impact of bauxite red mud disposal. *Mar. Pollut. Bull.* **2012**, *64*, 1895–1910. [CrossRef] [PubMed]
17. Liu, X.; Wang, Q.; Feng, Y.; Li, Z.; Cai, S. Genesis of the Guangou karstic bauxite deposit in western Henan, China. *Ore Geol. Rev.* **2013**, *55*, 162–175. [CrossRef]
18. Zhang, C.-Y.; Cao, P.; Pu, C.-Z.; Liu, J.; Wen, P.-H. Integrated identification method of rheological model of sandstone in Sanmenxia bauxite. *Trans. Nonferrous Met. Soc. China* **2014**, *24*, 1859–1865. [CrossRef]
19. Zhang, L.; Park, C.; Wang, G.; Wu, C.; Santosh, M.; Chung, D.; Song, Y. Phase transformation processes in karst-type bauxite deposit from Yunnan area, China. *Ore Geol. Rev.* **2017**, *89*, 407–420. [CrossRef]
20. Hou, T.; Zhang, L.; Yuan, Y.; Yang, Y.; Na, H. Review of the Chinese Aluminum Industry's Low-Carbon Development Driven by Carbon Tariffs: Challenges and Strategic Responses. *Processes* **2024**, *12*, 2707. [CrossRef]
21. Jégourel, Y. A Chequered African History of Commodity Markets, Part One: Bauxite and Aluminium. OCP Policy Centre PB-15 21, August 28, 2015. Available online: https://www.policycenter.ma/publications/chequered-african-history-commodity-markets-part-one-bauxite-and-aluminium (accessed on 10 July 2026).
22. Human Rights Watch. *"What Do We Get Out of It?"*; Human Rights Watch: New York, NY, USA, 2018; Available online: https://www.hrw.org/report/2018/10/04/what-do-we-get-out-it/human-rights-impact-bauxite-mining-guinea (accessed on 10 July 2026).
23. Wang, L. Quality Control Analysis of Ore from Open-Pit Mining of Sedimentary Bauxite in Xingxian County. *Chin. Min. Eng.* **2022**, *51*, 90–93.
24. Luo, J. *Research on the Strategic Development of China's Aluminum Industry Based on the Globalization of Bauxite Resources*; Central South University: Changsha, China, 2006.
25. Li, M.; Yang, C.; Wang, J. *The Mechanism of Water Inrush in Alumina Ore Deposits and Prevention Technologies The Theoretical and Practical Approaches to Water Inrush Control in Jiaogou Alumina Ore Deposit in Western Henan Province*; Huanghe Water Conservancy Press: Zhengzhou, China, 2007.
26. Peng, L.; Yang, X.; Sun, X. Analysis and control on anomaly water inrush in roof of fully-mechanized mining field. *Min. Sci.* **2011**, *21*, 89–92. [CrossRef]
27. Tingting, L.; Zhenhua, X. Work Safety Standardization Grade Evaluation Model and System Development of Bauxite Mines. *Procedia Eng.* **2011**, *26*, 1927–1933. [CrossRef]
28. Li, S.-C.; Zhou, Z.-Q.; Li, L.-P.; Xu, Z.-H.; Zhang, Q.-Q.; Shi, S.-S. Risk assessment of water inrush in karst tunnels based on attribute synthetic evaluation system. *Tunn. Undergr. Space Technol.* **2013**, *38*, 50–58. [CrossRef]
29. Cui, D. Analysis of Alumina Ore Mining Technology in Karst Areas. *Inn. Mong. Coal Econ.* **2015**, *5*, 7–8.
30. Li, J. *Research on Mine Water Control in the Deep Mining Conditions of Maoping Lead-Zinc Ore District in Northeastern Yunnan*; Kunming University of Science and Technology: Kunming, China, 2015.
31. Gao, S.; Wang, Z.; Zhang, R. Research on the Extraction Technology of Moderately Inclined Bauxite. *Non-Ferr. Met. Min. Sect.* **2016**, *68*, 3.
32. Wu, Y.; Li, X.; Yu, L.; Wang, T.; Wang, J.; Liu, T. Review of soil heavy metal pollution in China: Spatial distribution, primary sources, and remediation alternatives. *Resour. Conserv.* **2022**, *181*, 106261. [CrossRef]
33. Mahato, M.K.; Singh, G.; Singh, P.K.; Singh, A.K.; Tiwari, A.K. Assessment of Mine Water Quality Using Heavy Metal Pollution Index in a Coal Mining Area of Damodar River Basin, India. *Bull. Environ. Contam. Toxicol.* **2017**, *99*, 54–61. [CrossRef] [PubMed]
34. Tepanosyan, G.; Sahakyan, L.; Belyaeva, O.; Asmaryan, S.; Saghatelyan, A. Continuous impact of mining activities on soil heavy metals levels and human health. *Sci. Total Environ.* **2018**, *639*, 900–909. [CrossRef] [PubMed]
35. Steefel, C.; Depaolo, D.; Lichtner, P. Reactive transport modeling: An essential tool and a new research for earth sciences. *Earth Planet. Sci. Lett.* **2005**, *240*, 539–558. [CrossRef]
36. Fabre, G. Karst bauxites. Bauxite deposits on carbonate rocks G. Bardossy. Developments in economic geology n° 14, Elsevier sci. publi. campany, Amsterdam-Oxford-New York, 1982. *Karstologia* **1983**, *2*, 70–71. [CrossRef]
37. Noiriel, C.; Luquot, L.; Madé, B.; Raimbault, L.; Gouze, P.; van der Lee, J. Changes in reactive surface area during limestone dissolution: An experimental and modelling study. *Chem. Geol.* **2009**, *265*, 160–170. [CrossRef]
38. Crank, J. *The Mathematics of Diffusion*; Oxford University Press: Oxford, UK, 1979.
39. Levenspiel, O. *Chemical Reaction Engineering*; John Wiley & Sons: Hoboken, NJ, USA, 1998.
40. Nordstrom, D.K. Mine waters: Acidic to circmneutral. *Elements* **2011**, *7*, 393–398. [CrossRef]
41. Lottermoser, B.G. Mine water. In *Mine Wastes: Characterization, Treatment and Environmental Impacts*; Springer: Berlin/Heidelberg, Germany, 2010; pp. 119–203.
42. Zheng, X.; Lu, Y.; Xu, J.; Geng, H.; Li, Y. Assessment of heavy metals leachability characteristics and associated risk in typical acid mine drainage (AMD)-contaminated river sediments from North China. *J. Clean. Prod.* **2023**, *413*, 137338. [CrossRef]

43. Iepure, G.; Pop, A. Treatment of Acid Mine Water from the Breiner-Băiuț Area, Romania, Using Iron Scrap. *Water* **2025**, *17*, 225. [CrossRef]
44. Kortei, N.K.; Heymann, M.E.; Essuman, E.K.; Kpodo, F.M.; Akonor, P.T.; Lokpo, S.Y.; Boadi, N.O.; Ayim-Akonor, M.; Tettey, C. Health risk assessment and levels of toxic metals in fishes (*Oreochromis noliticus* and *Clarias anguillaris*) from Ankobrah and Pra basins: Impact of illegal mining activities on food safety. *Toxicol. Rep.* **2020**, *7*, 360–369. [CrossRef] [PubMed]
45. Larsson, M.; Nosrati, A.; Kaur, S.; Wagner, J.; Baus, U.; Nydén, M. Copper removal from acid mine drainage-polluted water using glutaraldehyde-polyethyleneimine modified diatomaceous earth particles. *Heliyon* **2018**, *4*, e00520. [CrossRef] [PubMed]
46. Dean, A.P.; Hartley, A.; McIntosh, O.A.; Smith, A.; Feord, H.K.; Holmberg, N.H.; King, T.; Yardley, E.; White, K.N.; Pittman, J.K. Metabolic adaptation of a Chlamydomonas acidophila strain isolated from acid mine drainage ponds with low eukaryotic diversity. *Sci. Total Environ.* **2019**, *647*, 75–87. [CrossRef] [PubMed]
47. Hammarstrom, J.; Seal, R.; Meier, A.; Kornfeld, J. Secondary sulfate minerals associated with acid drainage in the eastern US: Recycling of metals and acidity in surficial environments. *Chem. Geol.* **2005**, *215*, 407–431. [CrossRef]
48. Erasmus, J.; Malherbe, W.; Zimmermann, S.; Lorenz, A.; Nachev, M.; Wepener, V.; Sures, B.; Smit, N. Metal accumulation in riverine macroinvertebrates from a platinum mining region. *Sci. Total Environ.* **2020**, *703*, 134738. [CrossRef] [PubMed]
49. Younger, P.L.; Banwart, S.A.; Hedin, R.S. Mine water hydrology. In *Mine Water: Hydrology, Pollution, Remediation*; Springer: Dordrecht, The Netherland, 2002; pp. 127–270.
50. *12914:2012*; Soil Quality-Microwave-Assisted Extraction of the Aqua Regia Soluble Fraction for the Determination of Elements. International Organization for Standardization (ISO): Geneva, Switzerland, 2012.
51. Castaldi, P.; Silvetti, M.; Enzo, S.; Melis, P. Study of sorption processes and FT-IR analysis of arsenate sorbed onto red muds (a bauxite ore processing waste). *J. Hazard. Mater.* **2010**, *175*, 172–178. [CrossRef] [PubMed]
52. Goldberg, S.; Johnston, C.T. Mechanisms of arsenic adsorption on amorphous oxides evaluated using macroscopic measurements, vibrational spectroscopy, and surface complexation modeling. *J. Colloid Interface Sci.* **2001**, *234*, 204–216. [CrossRef] [PubMed]
53. Weng, L.; Van Riemsdijk, W.H.; Hiemstra, T. Factors controlling phosphate interaction with iron oxides. *J. Environ. Qual.* **2012**, *41*, 628–635. [CrossRef] [PubMed]
54. Miranda-Trevino, J.C.; Coles, C.A. Kaolinite properties, structure and influence of metal retention on pH. *Appl. Clay Sci.* **2003**, *23*, 133–139. [CrossRef]
55. Bhattacharyya, K.G.; Gupta, S.S. Adsorption of a few heavy metals on natural and modified kaolinite and montmorillonite: A review. *Adv. Colloid Interface Sci.* **2008**, *140*, 114–131. [CrossRef] [PubMed]
56. Zahedi, R.; Mirmohammadi, S.J. Sulfate removal from chemical industries' wastewater using ettringite precipitation process with recovery of Al (OH) 3. *Appl. Water Sci.* **2022**, *12*, 226. [CrossRef]
57. Lee, M.-K.; Saunders, J.A. Effects of pH on metals precipitation and sorption: Field bioremediation and geochemical modeling approaches. *Vadose Zone J.* **2003**, *2*, 177–185. [CrossRef]
58. Nordstrom, D.K.; Alpers, C.N. Geochemistry of acid mine waters. In *The environmental Geochemistry of Mineral Deposits*; Society of Economic Geologists: Littleton, CO, USA, 1997; pp. 133–160.
59. Aung, H.T.; Kolesnikov, A.V.; Averina, M.; Chelnokov, V.V.; Chyragov, F.M. Effect of background electrolytes and pH on electroflotation efficiency for heavy metal removal. *UNEC J. Eng. Appl. Sci.* **2025**, *5*, 115–123. [CrossRef]
60. Moncur, M.; Ptacek, C.; Blowes, D.; Jambor, J. Release, transport and attenuation of metals from an old tailings impoundment. *Appl. Geochem.* **2005**, *20*, 639–659. [CrossRef]
61. Acero, P.; Ayora, C.; Torrentó, C.; Nieto, J.-M. The behavior of trace elements during schwertmannite precipitation and subsequent transformation into goethite and jarosite. *Geochim. Cosmochim. Acta* **2013**, *70*, 4130–4139.
62. Dzombak, D.A.; Morel, F.M.M. *Surface Complexation Modeling: Hydrous Ferric Oxide*; John Wiley & Sons: Hoboken, NJ, USA, 1991.
63. Smedley, P.L.; Kinniburgh, D.G. A review of the source, behaviour and distribution of arsenic in natural waters. *Appl. Geochem.* **2002**, *17*, 517–568. [CrossRef]
64. Botsou, F.; Koutsopoulou, E.; Andrioti, A.; Dassenakis, M.; Scoullos, M.; Karageorgis, A. Chromium speciation, mobility, and Cr(VI) retention–release processes in ultramafic rocks and Fe–Ni lateritic deposits of Greece. *Environ. Geochem. Health* **2022**, *44*, 2815–2834. [CrossRef] [PubMed]
65. Raphulu, M.; Chauke, N.M.; Mapukata, S.; Mudzanani, K.; Maiga, D.; Phadi, T. Acid Mine Drainage Treatment and Control: Remediation Methodologies, Mineral Beneficiation and Water Reclamation Strategies. In *Hydrology—Current Research and Future Directions*; Murat, A.A.E., Alazaiza Motasem, Y.D., Eds.; IntechOpen: Rijeka, Croatia, 2024.
66. Cardwell, R.D.; DeForest, D.K.; Brix, K.V.; Adams, W.J. Do Cd, Cu, Ni, Pb, and Zn biomagnify in aquatic ecosystems? *Rev. Environ. Contam. Toxicol.* **2013**, *226*, 101–122. [CrossRef] [PubMed]
67. Skousen, J.G.; Sexstone, A.; Ziemkiewicz, P.F. Acid Mine Drainage Control and Treatment. *Reclam. Drastically Disturb. Lands* **2000**, *41*, 131–168. [CrossRef]
68. Herath, H.K.; Cizdziel, J.V.; Platt, B.F.; Widanagamage, I.H. Potential removal of heavy metal ions from polluted water using Bauxite. *Environ. Adv.* **2023**, *12*, 100362. [CrossRef]

69. Tian, T.; Wu, C.; Gong, L.; Yao, C.; Xiao, H.; Liu, L.; Li, F. Insights on Immobilization of Cd Contamination in Soil: Synergic Impacts of Water Management and Bauxite Residue. *ACS Omega* **2024**, *9*, 48497–48504. [CrossRef] [PubMed]
70. Equeenuddin, S.M.; Tripathy, S.; Sahoo, P.; Panigrahi, M. Metal behavior in sediment associated with acid mine drainage stream: Role of pH. *J. Geochem. Explor.* **2013**, *124*, 230–237. [CrossRef]
71. Alakangas, L.; Andersson, E.; Mueller, S. Neutralization/prevention of acid rock drainage using mixtures of alkaline by-products and sulfidic mine wastes. *Environ. Sci. Pollut. Res.* **2013**, *20*, 7907–7916. [CrossRef] [PubMed]
72. Lweya, C.; Jessen, S.; Banda, K.; Nyambe, I.; Koch, C.B.; Larsen, F. Groundwater transport of Cu in laterites in Zambia. *Appl. Geochem.* **2015**, *56*, 94–102. [CrossRef]
73. Gonçalves, N.P.; da Silva, E.F.; Tarelho, L.A.; Labrincha, J.A.; Novais, R.M. Simultaneous removal of multiple metal (loid) s and neutralization of acid mine drainage using 3D-printed bauxite-containing geopolymers. *J. Hazard. Mater.* **2024**, *462*, 132718. [CrossRef] [PubMed]
74. Babel, S.; Kurniawan, T.A. Low-cost adsorbents for heavy metals uptake from contaminated water: A review. *J. Hazard. Mater.* **2003**, *97*, 219–243. [CrossRef] [PubMed]

Disclaimer/Publisher's Note: The statements, opinions and data contained in all publications are solely those of the individual author(s) and contributor(s) and not of MDPI and/or the editor(s). MDPI and/or the editor(s) disclaim responsibility for any injury to people or property resulting from any ideas, methods, instructions or products referred to in the content.